

Formation of Co/Ge intermixing layers after Co deposition on Ge(111)2 × 1 surfaces

This article has been downloaded from IOPscience. Please scroll down to see the full text article.

2012 Nanotechnology 23 435605

(<http://iopscience.iop.org/0957-4484/23/43/435605>)

View [the table of contents for this issue](#), or go to the [journal homepage](#) for more

Download details:

IP Address: 93.180.54.107

The article was downloaded on 16/10/2012 at 15:46

Please note that [terms and conditions apply](#).

Formation of Co/Ge intermixing layers after Co deposition on Ge(111) 2×1 surfaces

D A Muzychenko¹, K Schouteden², V I Panov¹ and C Van Haesendonck²

¹ Faculty of Physics, Moscow State University, 119991 Moscow, Russia

² Laboratory of Solid-State Physics and Magnetism, KU Leuven, BE-3001 Leuven, Belgium

E-mail: mda@spmlab.ru

Received 14 June 2012, in final form 19 August 2012

Published 11 October 2012

Online at stacks.iop.org/Nano/23/435605

Abstract

The formation of a novel surface reconstruction upon Co deposition on freshly cleaved Ge(111) 2×1 surfaces is studied by means of scanning tunneling microscopy (STM) at 4.5 K. Previously we demonstrated that at this low substrate temperature the deposited Co atoms remain immobile after they become embedded underneath the Ge(111) 2×1 surface. We now demonstrate that at higher substrate temperatures the embedded Co atoms are able to diffuse below the surface in a direction parallel to the upper π -bonded chain rows. This one-dimensional temperature-induced mobility results in subsurface accumulation of Co atoms at atomic steps, at domain boundaries and on atomically flat Ge terraces at, e.g., vacancies or adatoms, where reconstructed Co/Ge intermixing layers are formed. Voltage dependent STM images reveal that the Co related surface reconstruction locally exhibits an ordered atomic structure with the same inter-atomic distance as that of the initial 2×1 reconstructed pure Ge(111) surface. On the other hand, the presence of the Co results in a doubling of the periodicity along the $[2\bar{1}\bar{1}]$ direction in the STM images, which can be related to the modified electronic properties of the π -bonded chains.

(Some figures may appear in colour only in the online journal)

1. Introduction

During the past few years impressive progress has been achieved by the nanoelectronics related research community in overcoming the difficulties that are encountered for future miniaturization of electronic devices down to the nanometer scale [1–3]. However, in order to further continue this miniaturization trend, new materials are needed with enhanced electronic properties when compared to those of silicon. In particular, higher electron and hole mobility may result in the use of the new materials for application in high-speed devices. Among the many different materials Ge is considered today as a promising alternative [4–6] because of its high carrier mobility and its compatibility with current Si based technology [7]. In this view metal/Ge and germanide/Ge bilayers have received considerable interest in

the past few years because they exhibit a Schottky barrier at the interface [8–11].

In analogy with the current Si based technology, where metal silicides (formed by thermal reaction of a metal layer with the Si substrate) are used to contact the source, drain, and gate regions of the transistors [10], metal germanides may be used for the production of self-aligned contacts [12–14]. However, only a fraction of these germanides has the potential to be used as electrical contacts, since the electrical resistance of the germanide phase must be low and needs to have a high thermal stability. A detailed overview of the subsequent germanide phases, which are formed during thermal reaction of Ge with various metals, has been provided by Gaudet *et al* [15]. Three materials of this list fulfil the required criteria: CoGe₂, NiGe and PdGe. The phase evolution of Co- and Ni-germanides as a function of temperature has previously been studied in great detail [16–18], as well as their

Schottky diode behavior [19–21]. Due to their low formation temperature and low resistivity NiGe and PdGe germanides are considered to be the main candidates for contacts in Ge channel devices [22].

The growth of magnetic thin films, clusters or nanowires on semiconducting surfaces may be exploited to design novel spin-based electronic devices [23, 24]. Spintronics requires the combined use of semiconducting and ferromagnetic materials in order to control the degree of electron spin polarization [25]. The combination of Co and Ge is considered as an important candidate for this purpose. Although the Co/Ge system has already been studied intensively [16, 26–34], the initial adsorption stage of Co atoms on Ge surfaces has not yet been investigated. A deeper understanding of combining ferromagnetic metals with semiconductors, in particular Co and Ge, in nanostructures is of significant technological and fundamental interest for future spintronic applications.

Here, we present a low-temperature (LT) scanning tunneling microscopy (STM) study of the initial growth stage of sub-monolayer coverages of Co deposited on Ge(111) surfaces. Clean Ge(111) surfaces are obtained by cleavage under ultra-high vacuum (UHV) conditions at room temperature (RT) and reveal the typical 2×1 reconstruction. Previously we found by combined STM experiments and density functional theory (DFT) based calculations that at lower temperatures deposited Co atoms can become embedded non-invasively into the Ge(111) 2×1 surface [35]. The key feature of our present work is the first experimental observation of subsurface migration of these individual, embedded Co atoms, which leads to the formation of large areas of new Co/Ge intermixed structures. We find that at RT and even around 80 K the embedded Co atoms are able to diffuse in a direction parallel to the upper π -bonded chains, i.e. in the $[0\bar{1}1]$ direction, and accumulate at atomic steps, domain boundaries, vacancies and adatoms to form mixed Co/Ge layers that reveal a novel surface reconstruction.

2. Experimental details

STM measurements were performed with a LT ultra-high vacuum (UHV) setup (Omicron Nanotechnology), consisting of a room-temperature sample preparation chamber and a LT STM measurement chamber. The operating pressure in the chambers is around 5×10^{-11} and 4×10^{-12} mbar, respectively. In order to optimize measurement stability, the LT UHV setup is decoupled from the building by a specially designed vibration isolation floor. Electrochemically etched tungsten tips were used in all experiments. The tips were cleaned *in situ* by repeated flashing above 2000 K in order to remove the surface oxide layer and additional contamination. The tip quality was routinely checked by acquiring atomic resolution images of the ‘herringbone’ reconstruction of the Au(111) surface [36–38]. All reported STM experiments are performed at liquid helium temperature ($T_{\text{sample}} \simeq 4.5$ K). STM topographic imaging was performed in constant current mode. Everywhere in the text the tunneling bias voltage V_t refers to the sample voltage, while the STM tip is virtually

grounded. Image processing was achieved using Nanotec WSxM [39].

The investigated Ge samples are doped with Ga at a low doping level of $N_{\text{Ga}} = 1$ to 2×10^{16} cm $^{-3}$, resulting in p-type conductivity with bulk resistivity $\rho_{\text{bulk}} \simeq 0.2$ Ω cm. $4 \times 1.5 \times 0.8$ mm 3 Ge bars with their long axis aligned with the [111] direction were cleaved *in situ* in the preparation chamber. For this purpose a lateral mechanical force is applied to one end of the Ge bar (i.e. perpendicular to the long axis), while the other end of the Ge bar is clamped at the sample plate. The force is gradually increased until the Ge bar spontaneously cleaves along one of its (111) planes, exposing the clean Ge(111) surface of the remaining part of the Ge bar that is clamped at the sample plate. The freshly cleaved samples were transferred within about 5 min to the STM measurement chamber. The cleaved Ge(111) 2×1 surfaces were observed to retain their cleanliness for 5–7 days in the LT STM measurement chamber.

The experiments consist of three stages. First, the clean 2×1 reconstructed surface of the freshly cleaved Ge single crystal is characterized in detail by STM measurements at $T_{\text{sample}} \simeq 4.5$ K [40]. Second, 0.02–0.04 monolayers (MLs) of Co atoms are deposited in the preparation chamber on the cold Ge surface (T_{sample} around liquid nitrogen temperature) by means of an electron-beam evaporator at a rate of 0.007 ± 0.001 MLs s $^{-1}$. A high purity Co (99.9996%) rod is used for the Co atom evaporation. Third, the Co containing Ge sample is again investigated in the LT STM measurement chamber, where it is further cooled down to about 4.5 K. For some of the LT STM measurements the Co containing Ge sample received an additional annealing at RT by again transferring the sample to the preparation chamber and then transferring it back to the LT STM measurement chamber. We carefully checked the possible influence on our STM measurements of surface contamination resulting from increasing the sample temperature to either temperatures around liquid nitrogen temperature or RT in between the STM measurements at liquid helium temperature [35, 40]. We found only very limited traces of surface contamination which can be clearly distinguished from the surface features on which we report based on the instabilities of the tunneling current at the small contaminated areas. On the other hand, we restricted the total measuring time for each of the investigated Ge(111) 2×1 surfaces to a maximum of 3 days to further restrict the influence of surface contamination.

3. Results and discussion

3.1. The freshly cleaved Ge(111) 2×1 surface

Prior to investigation of the Co related structures, a careful characterization of the clean Ge(111) 2×1 surface is obviously required. For this purpose we performed STM measurements on 7 freshly cleaved Ge crystals. After our analysis of atomic resolution STM topography images with size up to $1.9 \mu\text{m}^2$ of clean Ge(111) 2×1 surfaces, we conclude that the following surface structures exist after cleavage [35, 40]: (i) atomically flat terraces that exhibit the 2×1 surface reconstruction; (ii)

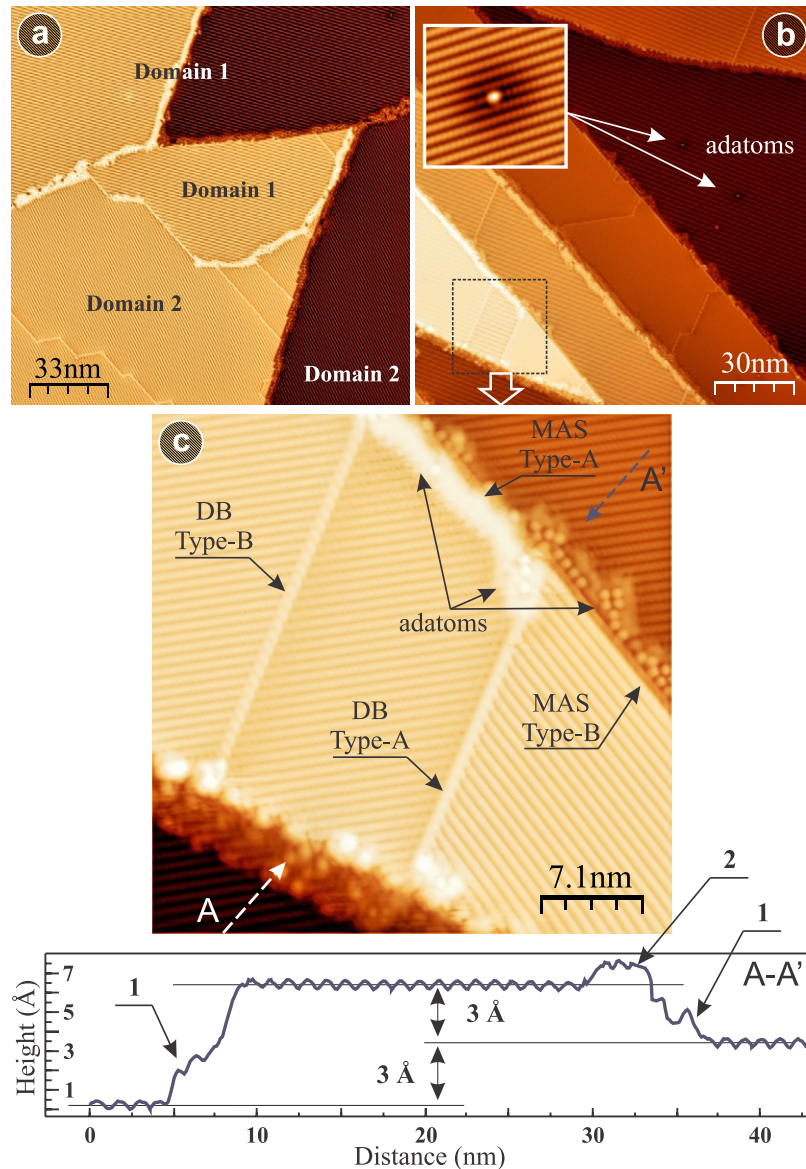


Figure 1. (a) and (b) Typical large-scale STM images of the freshly cleaved Ge(111) 2×1 surface ($V_t = +1.0$ V, $I_t = 20$ pA). The white arrows in (b) indicate the position of two Ge adatoms above a subsurface Ga impurity. (c) STM image of the area enclosed by the dotted black square in (b). The inset in (b) gives a 9×9 nm 2 close-up view of a Ge adatom located above a subsurface Ga impurity. (Bottom) Height profile taken along the line in between the two dashed arrows with labels A and A'.

monatomic steps (MASs) of type-A and type-B; (iii) domain boundaries (DBs) of type-A and type-B; (iv) Ge adatoms and vacancies; (v) Ga impurities and impurity/adatom complexes.

In figure 1 we present two typical large-scale STM images (figures 1(a) and (b)) and a high-resolution STM image (figure 1(c)) of the clean Ge(111) 2×1 surface. Large atomically flat terraces with size up to 10^5 nm 2 can be easily retrieved. The terraces are separated from each other by MASs and reveal the typical 2×1 reconstruction, consisting of π -bonded chains of Ge atoms [41–43] running in the $[01\bar{1}]$ direction. It is well known that only the upper chains are visualized by STM [44].

Figure 1 further reveals the presence of type-A and type-B DBs that separate different domains of the Ge(111) 2×1 surface [35, 40, 46]. For type-A DBs the chains at the

opposite sides of the DB are rotated by an angle of $\pi/3$, while type-B DBs are formed due to a shift of the π -bonded chains in the $[2\bar{1}\bar{1}]$ direction by half a unit cell (see figure 1(c)). In addition one recognizes in figures 1(a) and (c) the presence of both type-A and type-B MASs on the Ge(111) 2×1 surface [35]. For type-A MASs the π -bonded chains on the upper terrace are oblique to the MAS, while for type-B MASs the π -bonded chains on the upper terrace run parallel to the MAS. Ge adatoms are often present at these MASs (see figure 1(c)) [35, 43]. These Ge adatoms are created during cleavage at RT and they migrate along π -bonded chains to the MASs. In the STM images Ge adatoms at MASs appear as bright protrusions on top of the 2×1 surface reconstruction in the investigated voltage range between $V_t = -2.5$ and $+2.5$ V, as can be seen in the height profile in figure 1(c),

where the Ge adatoms at the lower and at the upper terraces near the type-A MAS are indicated by labels (1) and (2), respectively. Furthermore, (individual) Ge adatoms could be frequently observed at atomically flat Ge(111) 2×1 terraces and above features which we assign to charged subsurface Ga impurities (see the white arrows and the inset in figure 1(b) as well as the discussion of figure 1(a) in [40]). Subsurface Ga impurities locally modify the electronic properties of the 2×1 surface reconstruction, resulting in the appearance of a wider dark protrusion in the STM images at tunneling bias voltages above $V_t = +0.9$ V, independent of the presence/absence of a Ge adatom on top. The latter adatoms, which appear as small atomic size bright protrusions (see the inset in figure 1(b)) at all tunneling bias voltages, are well separated from each other and their number correlates with the low doping level of our Ge samples [35, 40].

3.2. Co deposition on cold Ge(111) 2×1 surfaces

Four freshly cleaved Ge crystals were investigated after Co atom deposition and surface areas of up to $2.4 \mu\text{m}^2$ were visualized by STM with atomic resolution. Figure 2 presents a typical large-scale STM image of the Ge(111) 2×1 surface after deposition of 0.032 ± 0.005 MLs of Co atoms on a cold Ge(111) 2×1 surface (T_{sample} around liquid nitrogen temperature). Apart from Co atoms that are uniformly distributed across the atomically flat Ge terraces, it can be seen that novel reconstructed structures are formed, e.g., at MASs and DBs. At higher positive sample voltages (empty-states images) these structures appear somewhat lower than the atomically flat terraces in the STM images and cover around 15% of the entire surface area and are referred to as Co/Ge intermixing layers (ILs) hereafter.

The close-up view in figure 3(a) comprises the three different types of Co related structures that can be observed after Co deposition on cold Ge(111) 2×1 surfaces (see [35] for a detailed discussion): (i) well separated individual Co atoms (label (1)); (ii) Co clusters consisting of multiple Co atoms (label (2)); (iii) Co/Ge ILs (label (3)).

First, a significant fraction of the deposited Co atoms ($13 \pm 5\%$) are retrieved as well separated individual atoms on the Ge(111) 2×1 surface. Single Co atoms appear as small bright protrusions in the STM images and are located at the upper π -bonded chains for voltages above 0.7 V (see figure 3(b)). A high-resolution STM image is presented in figure 3(c). Recently, we demonstrated that these Co atoms actually are not on top of the Ge(111) 2×1 surface, but penetrate into the Ge surface, where they occupy quasi-stable positions inside the big 7-member Ge rings of the 2×1 reconstruction between the 3rd and the 4th atomic layer below the surface [35]. The ‘embedding’ of Co atoms in the Ge surface significantly influences the local electronic structure, but it does not result in a modified surface reconstruction. As illustrated in figure 3(b), all individual Co atoms occupy identical positions. Consequently, all embedded Co atoms exhibit an identical electronic behavior and equally affect the electronic properties of the host π -bonded chains [35]. Second, small Co clusters consisting of a varying amount

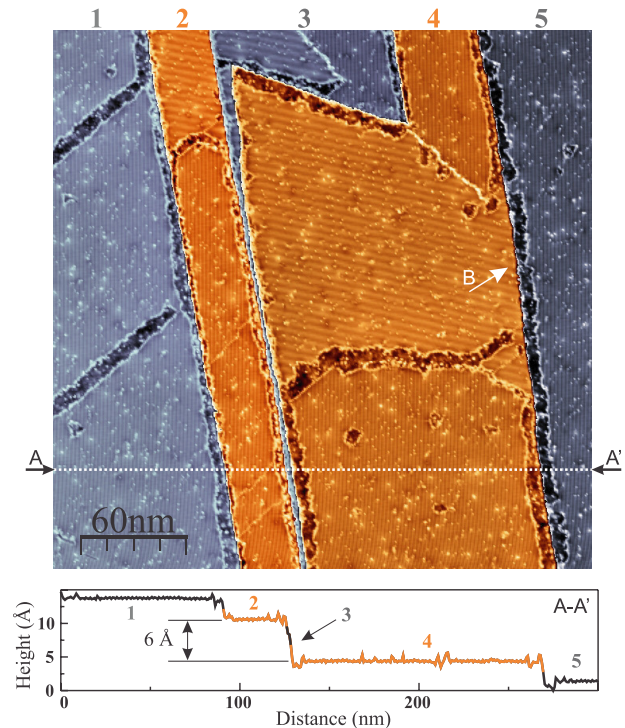


Figure 2. (Top) STM image of five Ge terraces after deposition of 0.032 ± 0.005 MLs of Co atoms on a cold (T_{sample} around liquid nitrogen temperature) Ge(111) 2×1 surface ($V_t = +1.0$ V and $I_t = 15$ pA). The white arrow B indicates the upper edge of a type-B MAS where no Co/Ge IL is formed (see discussion in section 3.3). (Bottom) Height profile taken along the white dotted line AA'.

of Co atoms with varying organization can occasionally be observed (figure 3(a)). These Co clusters may be partially embedded in the subsurface layers and the embedded Co atoms can then act as nucleation centers for further Co cluster growth. The clusters exhibit electronic properties that are strongly size dependent and are different from those of individual Co atoms.

Third, larger areas of a new type of Co related surface structures, the so-called Co/Ge ILs, can be observed after Co deposition on cold Ge surfaces (see the area enclosed by the two black dotted curves indicated by label (3) in figure 3(a)). These ILs together with the Co clusters comprise $87 \pm 5\%$ of the amount of deposited Co atoms. From the height profile in figure 3(d), which is taken along the line AA', it can be seen that these Co/Ge ILs appear about 1.2 \AA lower than the surrounding Ge terraces in STM images recorded at high positive voltages. This appearance differs from that of Ge adatom related structures (see section 3.1) and indicates a strongly modified electronic behavior of the Co/Ge IL when compared to the surrounding 2×1 reconstruction. We found that Co/Ge ILs nucleate at three different surface locations: (i) at MASs (see figures 4(a) and (c)), (ii) at DBs (see figure 3 and 4(c)) and (iii) on atomically flat Ge(111) terraces at, e.g., vacancies or adatoms (see figure 4(b)). It must be noted that for the type-A MASs Co/Ge ILs are formed at both the upper and the lower terraces (figure 4(a)), whereas for type-B MASs Co/Ge ILs are formed at the lower terrace only (see figure 4(c)). For DBs of both type-A and type-B

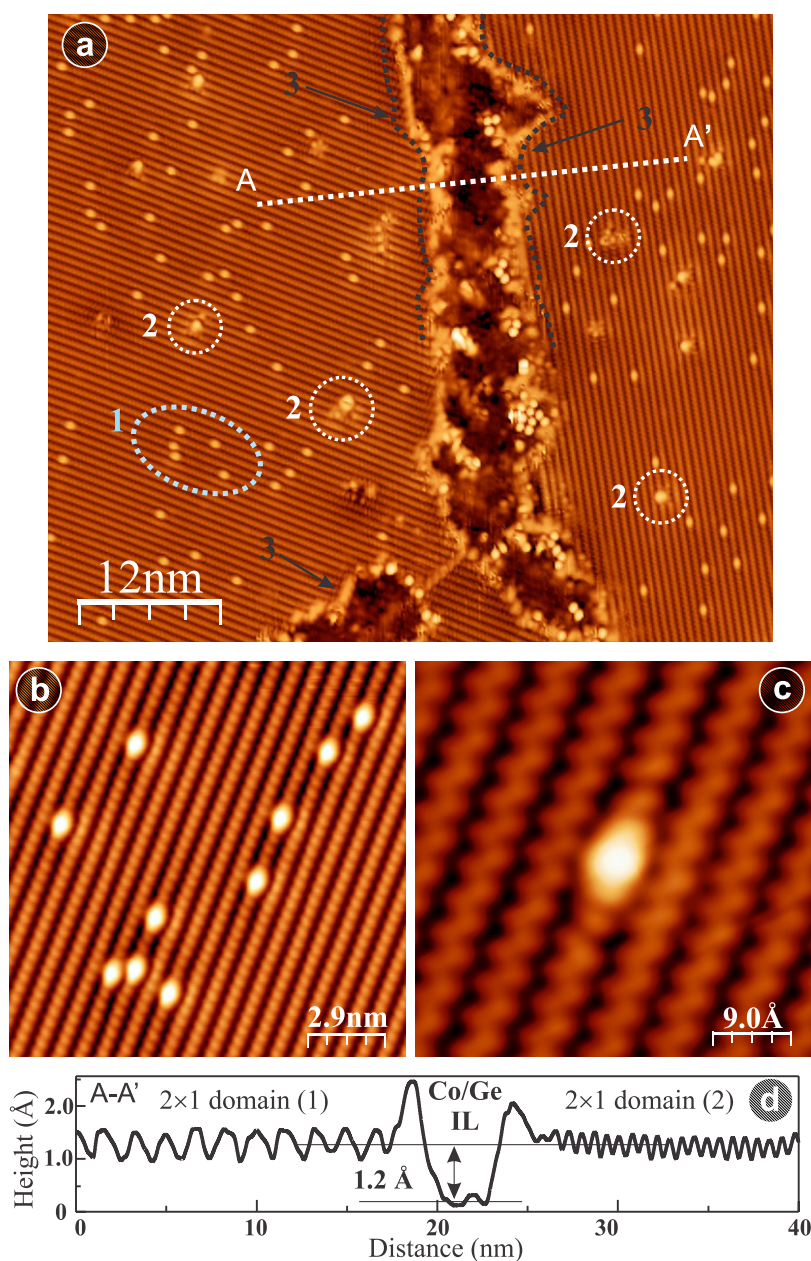


Figure 3. (a) STM image of the Ge(111) 2×1 surface after Co deposition ($V_t = +1.0$ V, $I_t = 15$ pA). Three different Co related structures can be retrieved: (1) individual Co atoms that are embedded in the Ge(111) 2×1 surface in between the 3rd and 4th atomic layer underneath the surface, (2) Co clusters consisting of multiple atoms and (3) areas of Co/Ge intermixing layers. (b) STM image of 10 well separated individual Co atoms ($V_t = +1.0$ V, $I_t = 100$ pA). (c) Close-up view of an individual Co atom ($V_t = +0.9$ V, $I_t = 300$ pA). (d) Height profile taken along the line AA' across two different domains of the Ge surface that are separated by a Co/Ge intermixing layer.

Co/Ge ILs are formed at both sides of the DB. This can be clearly seen in figure 3(a), where a part of the unperturbed type-B DB can still be discerned at the bottom of the STM image. Co/Ge ILs formed at a type-A DB between two surface domains with different directions of the 2×1 reconstruction can also be observed in figure 3(a) (indicated by label (3)). Finally, Co/Ge ILs can be formed on Ge(111) 2×1 terraces as well (figure 4(b)). In the latter case atomic size surface features such as Ga dopant impurities or Ge vacancies trap incoming diffusing Co atoms and act as nucleation centers for the formation of two-dimensional (2D) Co/Ge ILs.

3.3. Formation of the Co/Ge intermixing layer

We now discuss in more detail the formation mechanism of the Co/Ge ILs. Clearly, the size of a Co/Ge IL depends on the size of the neighboring single-domain Ge(111) 2×1 terrace, as can be observed in figure 2 and in figure 4(a). For example, for the case of Co/Ge ILs formed at the MASs in figure 2, the width of the Co/Ge IL (measured perpendicular to the MAS) on the narrow Ge terrace (2) is much smaller than the width of the Co/Ge IL formed on the wide Ge terrace (5). Note that all MASs in figure 2 are of type-A, except for the middle part of terrace (4). The (relative) total area of the Co/Ge IL on the

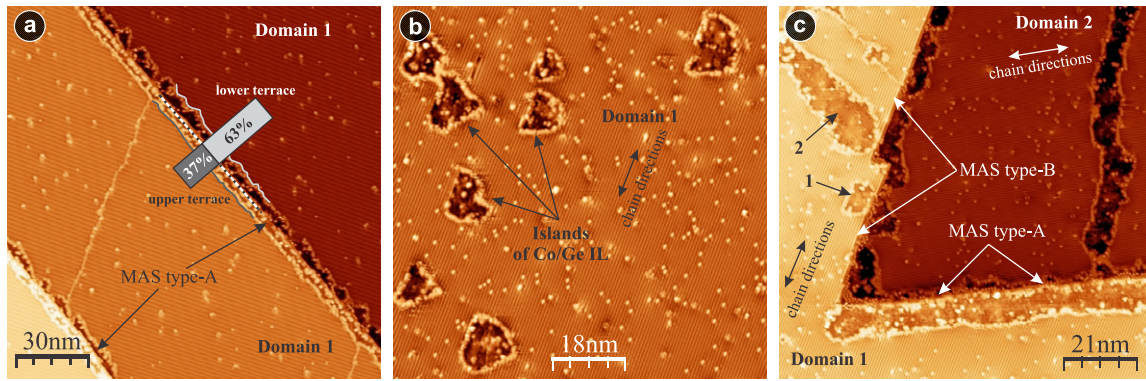


Figure 4. Co/Ge ILs nucleate at three different surface locations, i.e., at (a) MASs, (b) on atomically flat Ge terraces at, e.g., vacancies or adatoms and (c) at DBs ($V_t = +1.0$ V, $I_t = 15$ pA). Labels 1 and 2 in (c) indicate Co/Ge ILs formed at a type-B MAS.

upper and lower terraces at the MAS indicated in figure 4(a) is around $37 \pm 5\%$ and $63 \pm 5\%$, respectively. This is in agreement with the ratio of 1.9 ± 0.1 between the widths of the lower and upper terrace (which is inferred from large-scale STM images). Similarly, Ge terraces at MASs with an even larger difference in terrace width were found to yield larger differences in the formed IL areas as well. A more detailed analysis of the dependence of Co/Ge ILs on the width of the neighboring (single-domain) Ge terraces indicates, however, a nonlinear dependence. This can be accounted for by the fact that a fraction of the deposited Co atoms contributes to the formation of Co/Ge ILs at DBs and on atomically flat Ge terraces at vacancies or adatoms (see figures 2 and 4(b)).

As already noted above, Co/Ge ILs are not formed at the upper terraces of type-B MASs (see, e.g., the middle part of terrace (4) indicated by the white arrow with label B in figure 2). Figure 2 exhibits pronounced Moiré fringes that run along one direction and become visible because of the large size of the image, while the π -bonded chain rows of the 2×1 reconstruction remain invisible in the STM image. The π -bonded chains of the middle part of terrace (4) are oriented parallel to the neighboring MAS, which is consistent with the fact that the Co/Ge ILs are formed by diffusion of deposited Co atoms along the π -bonded chains, until they are immobilized at, e.g. a MAS or a DB. The strong anisotropy of the Ge(111) 2×1 surface reconstruction with respect to the $[01\bar{1}]$ and $[2\bar{1}\bar{1}]$ directions [42, 45] results in a preferred direction for one-dimensional migration of the Co atoms, i.e., along the π -bonded chains. It can indeed be seen in figure 4(c) that the upper terrace, forming both a type-A MAS and a type-B MAS, reveals the presence of a continuous Co/Ge IL at the type-A MAS. On the other hand, Co/Ge ILs at the type-B MAS (indicated by labels (1) and (2) in figure 4(c)) are formed only locally (and may be rather caused by the presence of a vacancy/adatom (1) and a DB (2)). Most of the upper terrace remains unaltered near this type-B MAS. Ge adatoms that exist after cleavage of the Ge crystal reveal a similar diffusion behavior on (clean) Ge(111) 2×1 surfaces (see figure 1(c) and section 3.1).

Next, we investigated the influence of the substrate temperature on the diffusion behavior of the deposited Co atoms and hence on the formation of the Co/Ge ILs. For

this purpose the temperature of the Co/Ge(111) 2×1 sample (with 0.032 ± 0.005 MLs of Co) was increased up to RT for 24 h, after which it was cooled down again to 4.5 K. In figures 5(a)–(c) we present three STM images of the Co/Ge(111) 2×1 surface recorded after this RT annealing procedure. The individual Co atoms, which were previously present at atomically flat Ge(111) 2×1 terraces (see figures 3 and 4) can no longer be observed. At the same time the area of the Co/Ge ILs (figures 5(a) and (b)) as well as the amount of Co clusters (figure 5(c)) increases. Since only $13 \pm 5\%$ of the total amount of deposited Co atoms is retrieved as individual Co atoms on Ge terraces (before warming up the sample), the increase of the total Co/Ge IL area and the amount of Co clusters (after warming up the sample) cannot be accurately determined. Nevertheless, we conclude that the mobility of the individual Co atoms increases when increasing the sample temperature to RT. This is, however, remarkable in view of the fact that the individual Co atoms are actually embedded in the Ge surface after deposition, i.e., in between the 3rd and the 4th Ge layer below the surface [35]. During embedding of the Co atom in the Ge(111) 2×1 surface, a potential barrier with height $\Delta E \simeq 0.5$ eV has to be overcome [35]. This implies that these Co atoms cannot gain sufficient energy by warming the sample up to RT to return back to the surface ($k_B T \simeq 25$ meV at RT). Migration of the embedded individual Co atoms at RT must therefore occur below/inside the Ge surface. The big 7-member Ge rings, which exist along π -bonded chains in the $[01\bar{1}]$ direction, appear to provide the only possible ‘route’ for this subsurface migration. As already discussed above, both Co/Ge ILs ($87 \pm 5\%$, including the occasionally observed Co clusters) and single Co atoms ($13 \pm 5\%$) are observed after Co atom deposition on cold Ge(111) 2×1 surfaces (T_{sample} around liquid nitrogen temperature), from which it can be concluded that the majority of the deposited Co atoms already have a sufficiently high mobility around liquid nitrogen temperature to diffuse along π -bonded chains in the $[01\bar{1}]$ direction. Above this temperature most of the atoms will be involved in the formation of Co/Ge ILs and Co clusters, while the amount of individual Co atoms increases with decreasing temperature below this temperature. Recently it has been demonstrated that subsurface intermixing layers are formed at semiconductor surfaces by diffusion and migration

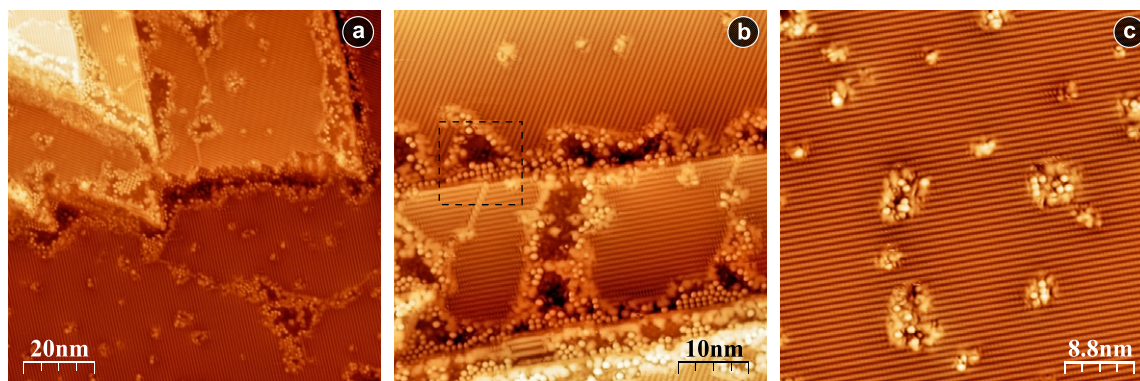


Figure 5. Empty-states STM images of the Co/Ge(111) 2×1 system recorded at 4.5 K after warming the sample up to RT for 24 h. Images are recorded at (a) $V_t = +1.0$ V and $I_t = 10$ pA, (b) $V_t = +0.87$ V and $I_t = 35$ pA, and (c) $V_t = +1.0$ V and $I_t = 20$ pA. The dashed black square in (b) indicates the scanned area for the STM images in figure 6.

of adsorbed atoms. For example, it has been shown both experimentally and theoretically that deposited Ge atoms diffuse to the 4th subsurface Si layer for Si(100) surfaces at a temperature of 500 °C [47]. Similarly, Si atoms deposited on Ge(100) 2×1 surfaces at RT have been found to move below the Ge surface [48]. Also, it has been demonstrated experimentally that an intermixing layer is formed when depositing Co on a Ge(111) surface at RT. Using MeV ion channeling and Auger electron spectrometry it has been found that for a Co coverage up to 3 MLs a thin layer of mixed Co and Ge is formed [49], which is consistent with our results.

In summary, we can state that the Co/Ge ILs are formed by subsurface accumulation of Co atoms at MASs, DBs and on atomically flat Ge terraces at, e.g., vacancies and adatoms. The accumulation results from one-dimensional subsurface migration of Co atoms through the 7-member Ge rings of the π -bonded chains in between the 3rd and the 4th atomic layer below the surface, yielding spatially extended 2D Co/Ge ILs as observed in our STM experiments.

3.4. Structure of the Co/Ge intermixing layer

At first sight the Co/Ge ILs may seem to be rather disordered, without any clear periodicity. However, from a detailed analysis of voltage dependent STM images we found that Co/Ge ILs exhibit an ordered atomic structure that can be revealed only at low tunneling bias voltages. In figures 6(a), (b) and (c), (d) we present empty-states and filled-states STM images, respectively, of a Co/Ge IL formed at a type-B MAS. The STM image was recorded at the location enclosed by the black dashed square in figure 5(b). As a guide to the eye the same group of adatoms is indicated by black crosses in figure 6.

Remarkably, the Co/Ge IL and the surrounding 2×1 reconstructed surface have about the same height at low voltages in the filled-states regime close to the Fermi energy E_F (figures 6(c) and (d)), while there appears to be a pronounced height difference of around 1.2 Å at higher voltages (see height profile in figure 3(d)). This voltage dependent behavior can be related to a change of the electronic properties of the π -bonded chains at the surface, rather than

to a change of the Ge(111) surface reconstruction. Moreover, the Co/Ge IL at the lower terrace in figure 6(d) (top part of the STM image) reveals, besides multiple adatoms, a locally ordered atomic structure with the same periodicity as that of the original 2×1 reconstruction along the π -bonded chains. Along the $[2\bar{1}\bar{1}]$ direction, i.e. perpendicular to the π -bonded chains, this new Co/Ge IL reconstruction has a ‘double periodicity’ when compared to the pure Ge(111) 2×1 surface.

In figure 7(a) we present a filled-states STM image of a Co/Ge IL formed at the lower terrace of another type-B MAS. This surface has not been warmed up to RT, implying that single Co atoms can still be observed in the empty-states STM image in figure 7(d). A close-up view of the area confined by the white solid and black dashed squares in figure 7(a) is presented in figure 7(b) (filled-states regime) and in figure 7(d) (empty-states regime), respectively. In figures 7(c) and (e) we present two atomic resolution STM images of the Co/Ge IL and the surrounding Ge(111) 2×1 surface. Although the Co/Ge ILs in general appear to be rather disordered, they locally exhibit an ordered atomic structure (figure 7(c)), which indicates that these ordered structures of the Co/Ge ILs are already formed at lower temperatures, prior to warming up to RT.

The local atomic structure of a Co/Ge IL can be visualized in more detail by relying on 2D Fourier transformation. This ‘double period’ of the atomic rows can be seen more clearly in figure 8(a), which is the 2D Fourier transform image of figure 7(b). The Bragg maxima originating from the 2×1 surface reconstruction in both the $[01\bar{1}]$ and the $[2\bar{1}\bar{1}]$ direction (indicated by the dotted and dashed arrows) can be clearly observed. Moreover, two additional maxima, which are related to the doubling of the periodicity in the $[2\bar{1}\bar{1}]$ direction due to the appearance of an additional row of atoms, can be nicely resolved (indicated by circles in figure 8(a)). In figure 8(b) we present the inverse Fourier transform image of the 6 Bragg maxima that are indicated in figure 8(a). In this Fourier filtered image the different atomic structures of the Co/Ge IL and the Ge(111) 2×1 surface are clearly resolved. The right-hand part of figure 8(b) corresponds to the Ge(111) 2×1 surface, while the left-hand part corresponds

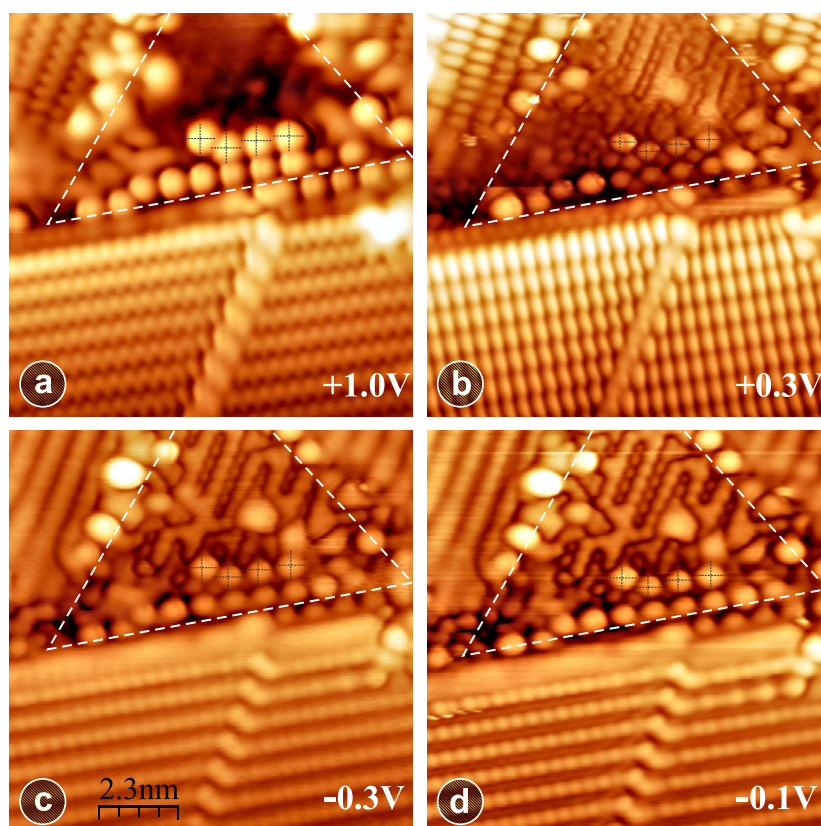


Figure 6. (a), (b) Empty-states and (c), (d) filled-states STM images of a Co/Ge IL (indicated by the white dashed triangle) formed at a type-B MAS, recorded at the location enclosed by the black dashed square in figure 5(b). The tunneling voltage is indicated for each of the images ((a)–(c) $I_t = 200$ pA and (d) $I_t = 50$ pA). As a guide to the eye the positions of four adatoms on the Co/Ge IL are indicated by black crosses in each of the STM images.

to a perfect (without any defects such as adatoms) Co/Ge IL surface reconstruction. It must be noted that the relative brightness of the ‘additional’ row of atoms with respect to the other row of atoms depends on the tunneling bias voltage, i.e. this brightness decreases with increasing voltage.

We now turn to the atomic structure which is able to provide a consistent explanation of our experimental results. In figure 9 we schematically present the atomic structure of the Ge(111) 2×1 surface as well as the position of a Co atom that is embedded within a big 7-member Ge ring. This scheme is based on our earlier DFT based calculations [35]. The atomic structure in figure 9 does not take into account possible relaxation of the surface π -bonded chains and Co atoms inside big 7-member Ge rings. Dotted lines indicate the different directions to the neighboring Ge atoms which are involved in chemical bond formation with the Co atom. Based on the atomic structure in figure 9 we can link the subsurface one-dimensional diffusion of Co atoms parallel to the π -bonded chain rows to the motion of Co atoms that move between adjacent big 7-member rings in the $[01\bar{1}]$ direction. The observed IL formation can be consistently related to this one-dimensional diffusion of Co atoms which results in accumulation of Co atoms at MASs, DBs or defects to form the Co/Ge ILs. Consequently, at these locations Co atoms become densely packed inside the big 7-member Ge rings along the upper π -bonded chain, while the 5-member Ge rings

of the neighboring lower π -bonded chains remain empty. We may then assume that the 2D Co/Ge ILs consist of alternating Co nanowires (with a periodicity of 0.69 nm) that are located in between the 3rd and 4th atomic layer below the Ge(111) 2×1 surface. The experimentally observed irregular structures on top of the Co/Ge ILs can be related to the Co atom deposition process. Already during the deposition process, deposited Co atoms are migrating and are hence forming the Co/Ge ILs. When a Co atom is then deposited on top of an already formed Co/Ge IL, it will become immobilized on the surface and will be observed as a Co adatom on the Co/Ge IL in the STM images (see figures 6 and 7). In addition, one needs to take into account that the formation of the Co/Ge ILs initially occurs at low temperature, implying that the mobility of the Co atoms in the subsurface Ge layers is strongly reduced (when compared to RT), which may hamper the formation of perfectly ordered Co/Ge ILs due to the presence of ‘holes’.

In the absence of the Co atoms the surface unit cell contains two atoms, both having one dangling bond that is responsible for π -bonding along the surface upper chains. Due to buckling one of these two atoms (referred to as the *up*-atom) is shifted somewhat out of the surface while the other (referred to as the *down*-atom) is shifted into the surface [45]. The occupied surface states are mainly localized on the *up*-atom, while the empty surface states are mainly localized on the *down*-atom of the π -bonded chain.

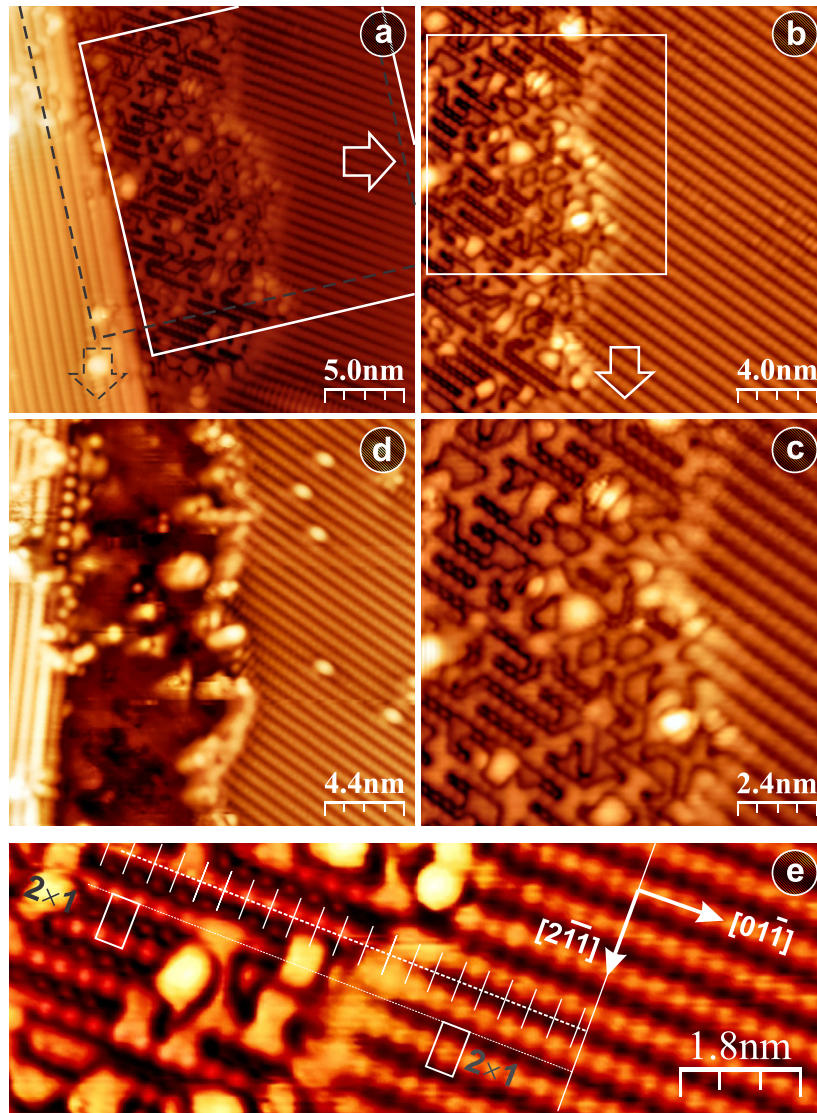


Figure 7. (a) Filled-states STM image of the Ge/Co IL formed at a type-B MAS ($V_t = -0.4$ V, $I_t = 50$ pA). (b), (c) Filled-states ($V_t = -0.4$ V, $I_t = 200$ pA) and (d) empty-states ($V_t = 1.0$ V, $I_t = 100$ pA) close-up views of the area enclosed by the white solid square in (a), the white solid square in (b) and the black dashed square in (a), respectively. (e) Atomic resolution STM image of the Co/Ge IL (left) and the Ge(111) 2×1 surface (right) at the type-B MAS ($V_t = -0.4$ V, $I_t = 50$ pA).

Consequently, the bonding surface states band derived from the *up*-atom orbital is filled, while the anti-bonding surface states band derived from the *down*-atom orbital is empty. These bands play an important role in the visualization of the Ge surface by STM images [50]. The presence of embedded Co atoms in the Ge surface implies bonding between the Co atom and the Ge *up*-atoms and the Ge *down*-atoms. As a result of the Co–Ge orbital hybridizations both dangling bonds are absent and a surface state is no longer present at the upper π -bonded chains in the Co/Ge IL. Since both surface states play a significant role in the STM image formation, their absence will result in a reduced (increased) contribution of the upper (lower) π -bonded chains to the tunneling current that determines the STM images at both polarities of the tunneling bias voltage. The contour of constant local density of states integrated over an energy range from E_F to $E_F + V_t$ (the tunneling bias voltage -0.5 V $< V_t < +0.5$ eV) can be

calculated using our DFT based simulations [35] and is given by the black dotted line in figure 9. In the presence of the Co atoms both atomic rows can be resolved in the STM images, i.e. the period of the atomic rows along the $[2\bar{1}\bar{1}]$ direction appears to have ‘doubled’ on the Co/Ge IL when compared to the surrounding Ge surface (figures 6(b)–(d) and 7(a)–(c)).

The structural changes imposed by the presence of the Co atoms can be observed more clearly in figure 7(e). The higher atomic rows of the reconstructed Co/Ge IL in the $[01\bar{1}]$ direction run parallel to the lower π -bonded chains of the Ge(111) 2×1 surface (see white dotted scale bar in figure 7(e)). The higher atomic rows of both regions are thus shifted by half of the total period along the $[2\bar{1}\bar{1}]$ direction with respect to each other. The surface unit cell of the Ge(111) 2×1 reconstruction is presented in figure 7(e) as well as the same surface unit cell shifted by 15 periods along the $[01\bar{1}]$ direction. It can be seen that, after this

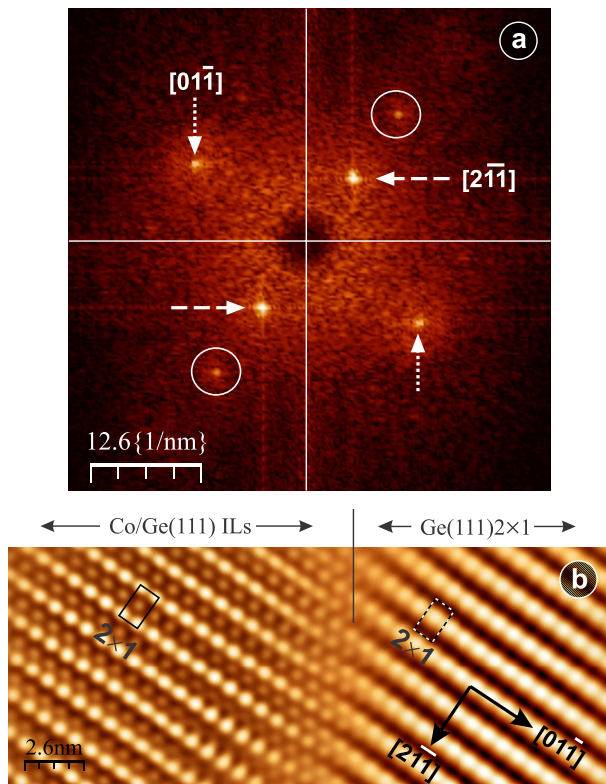


Figure 8. (a) 2D Fourier transform image of figure 7(b). The bright Bragg maxima indicated by the dotted and dashed arrows stem from the main periodicities of the $\text{Ge}(111)2 \times 1$ surface reconstruction. The two maxima indicated by circles stem from the double periodicity in the $[2\bar{1}\bar{1}]$ direction of the Co/Ge IL surface reconstruction. (b) Inverse Fourier transform (Fourier filtered) image of the 6 maxima indicated in (a).

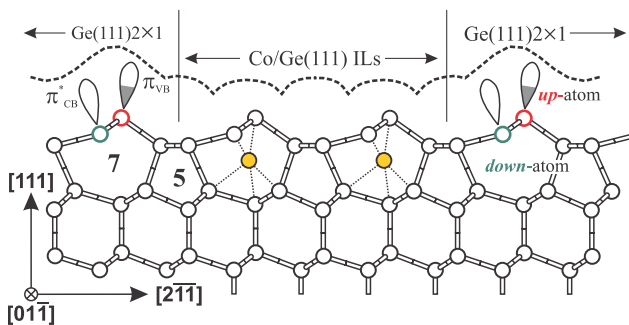


Figure 9. Schematic side view of the 2×1 reconstruction of the $\text{Ge}(111)$ surface (outer left and outer right part) and of the atomic structure of the Co/Ge(111) IL formed within two 7-member Ge rings (middle part). The locations of the Co atoms are indicated by the solid yellow circles, while dotted lines indicate the different directions to the neighboring Ge atoms. The numbers 7 and 5 indicate the 7-member and 5-member Ge rings, respectively. The black dotted line represents a contour of constant integrated local density of states (see text).

shift, the local minima at the corners of the surface unit cell on the clean $\text{Ge}(111)2 \times 1$ surface now correspond to the local maxima of the Co/Ge IL. Similarly, the local maxima of the $\text{Ge}(111)2 \times 1$ reconstruction (i.e., the Ge *up*-atoms) correspond to the local maxima of the (lower lying)

‘secondary period’ of the Co/Ge IL 2×1 reconstruction (see white dotted scale bar in figure 7(e)). Clearly, the new 2×1 reconstruction of the Co/Ge IL perfectly matches the periodicity of both the upper and lower π -bonded chains of the clean $\text{Ge}(111)2 \times 1$ surface in the $[01\bar{1}]$ direction. However, as already discussed above, the periodicity doubles along the $[2\bar{1}\bar{1}]$ direction due to the modified contributions of the upper and lower π -bonded chains to the STM images. A full understanding of the Co induced reconstruction requires detailed DFT based calculations, which are clearly beyond the scope of our current research and will be part of our future research.

4. Conclusions

We investigated by means of voltage dependent STM measurements at low temperature the adsorption of Co atoms on cold cleaved $\text{Ge}(111)2 \times 1$ surfaces (T_{sample} around liquid nitrogen temperature) for sub-monolayer Co coverage. Individual Co atoms, small Co clusters and Co/Ge intermixing layers (ILs) are retrieved on the Ge surface. Relying on DFT based calculations we recently demonstrated that the individual Co atoms become embedded into the $\text{Ge}(111)2 \times 1$ surface, in between the 3rd and 4th atomic layer below the surface. Here, we demonstrated that the embedded Co atoms are able to migrate (even at low temperatures) below the Ge surface to monatomic steps, domain boundaries, vacancies and adatoms, which act as nucleation centers for the formation of Co/Ge ILs. When the substrate is warmed up to RT, the mobility of the individual Co atoms further increases and all of them contribute to the formation of the Co/Ge ILs. The 2D Co/Ge ILs are formed by accumulation of subsurface Co atoms that migrate along the upper π -bonded chains. The ILs (locally) have an ordered atomic structure with the same inter-atomic distance as that of the initial 2×1 reconstruction in both the $[01\bar{1}]$ direction and the $[2\bar{1}\bar{1}]$ direction. However, the presence of the Co atoms results in the appearance of a double periodicity along the $[2\bar{1}\bar{1}]$ direction in the STM images due to the modified electronic properties of the upper and lower π -bonded chains.

Acknowledgments

The research in Moscow has been supported by the Russian Foundation for Basic Research (RFBR). The research in Leuven has been supported by the Fund for Scientific Research—Flanders (FWO, Belgium) as well as by the Flemish Concerted Research Action (GOA) and the Belgian Interuniversity Attraction Poles (IAP) research programs. KS is a postdoctoral researcher of the FWO. We thank S V Savinov for his technical support and for providing the Ge crystals.

References

- [1] Haider M B, Pitters J L, DiLabio G A, Livadaru L, Mutus J Y and Wolkow R A 2009 Controlled coupling and occupation of silicon atomic quantum dots at room temperature *Phys. Rev. Lett.* **102** 046805

- [2] Tan K Y *et al* 2009 Transport spectroscopy of single phosphorus donors in a silicon nanoscale transistor *Nano Lett.* **10** 11–5
- [3] Parks J J *et al* 2010 Mechanical control of spin states in spin-1 molecules and the underscreened Kondo effect *Science* **328** 1370–3
- [4] Chui C O, Gopalakrishnan K, Griffin P B, Plummer J D and Saraswat K C 2003 Activation and diffusion studies of ion-implanted p and n dopants in germanium *Appl. Phys. Lett.* **83** 3275–7
- [5] Bracht H, Schneider S, Klug J N, Liao C Y, Hansen J L, Haller E E, Larsen A N, Bougeard D, Posselt M and Wündisch C 2009 Interstitial-mediated diffusion in germanium under proton irradiation *Phys. Rev. Lett.* **103** 255501
- [6] Wündisch C *et al* 2009 Millisecond flash lamp annealing of shallow implanted layers in Ge *Appl. Phys. Lett.* **95** 252107
- [7] Sze S M and Irvin J C 1968 Resistivity, mobility and impurity levels in GaAs, Ge, and Si at 300 K *Solid-State Electron.* **11** 599–602
- [8] Rowe J E, Christman S B and Margaritondo G 1975 Metal-induced surface states during Schottky-barrier formation on Si, Ge, and GaAs *Phys. Rev. Lett.* **35** 1471–5
- [9] Chang Y, Hwu Y, Hansen J, Zanini F and Margaritondo G 1989 Nature of the Schottky term in the Schottky barrier *Phys. Rev. Lett.* **63** 1845–8
- [10] Byoung H L, Jungwoo O, Hsing H T, Rajarao J and Howard H 2006 Gate stack technology for nanoscale devices *Mater. Today* **9** 32–40
- [11] Tse K-Y and Robertson J 2007 Control of Schottky barrier heights on high-*k* gate dielectrics for future complementary metal–oxide semiconductor devices *Phys. Rev. Lett.* **99** 086805
- [12] Zhu S, Li R, Lee S J, Li M F, Du A, Singh J, Zhu C, Chin A and Kwong D L 2005 Germanium pMOSFETs with Schottky-barrier germanide S/D, high-*k* gate dielectric and metal gate *IEEE Electron Device Lett.* **26** 81–3
- [13] Park K, Lee B H, Lee D, Ko D H, Kwak K H, Yang C-W and Kim H 2007 A study on the thermal stabilities of the NiGe and Ni(1-*x*)Ta(*x*)Ge systems *J. Electrochem. Soc.* **154** H557–60
- [14] Brunco D P *et al* 2008 Germanium MOSFET devices: Advances in materials understanding, process development, and electrical performance *J. Electrochem. Soc.* **155** H552–61
- [15] Gaudet S, Detavernier C, Kellock A J, Desjardins P and Lavoie C 2006 Thin film reaction of transition metals with germanium *J. Vac. Sci. Technol. A* **24** 474–85
- [16] Ashburn S P, Öztürk M C, Harris G and Maher D M 1993 Phase transitions during solid-state formation of cobalt germanide by rapid thermal annealing *J. Appl. Phys.* **74** 4455–60
- [17] Gaudet S, Detavernier C, Lavoie C and Desjardins P 2006 Reaction of thin Ni films with Ge: phase formation and texture *J. Appl. Phys.* **100** 034306
- [18] Opsomer K, Deduytsche D, Detavernier C, Van Meirhaeghe R L, Lauwers A, Maex K and Lavoie C 2007 Influence of Ge substrate crystallinity on Co germanide formation in solid-state reactions *Appl. Phys. Lett.* **90** 031906
- [19] Chi D Z, Lee R T P, Chua S J, Lee S J, Ashok S and Kwong D L 2005 Current–voltage characteristics of Schottky barriers with barrier heights larger than the semiconductor band gap: the case of NiGe/n-(001)Ge contact *J. Appl. Phys.* **97** 113706
- [20] Simoen E, Opsomer K, Claeys C, Maex K, Detavernier C, Van Meirhaeghe R L, Forment S and Clauws P 2006 Deep level transient spectroscopy study of nickel-germanide Schottky barriers on n-type germanium *Appl. Phys. Lett.* **88** 183506
- [21] Simoen E, Opsomer K, Claeys C, Maex K, Detavernier C, Van Meirhaeghe R L and Clauws P 2008 Study of metal-related deep-level defects in germanide Schottky barriers on n-type germanium *J. Appl. Phys.* **104** 023705
- [22] Kittl J A, Opsomer K, Torregiani C, Demeurisse C, Mertens S, Brunco D P, Van Dal M J H and Lauwers A 2008 Silicides and germanides for nano-CMOS applications *Mater. Sci. Eng. B* **154** 144–54
- [23] Wolf S A, Awschalom D D, Buhrman R A, Daughton J M, von Molnar S, Roukes M L, Chtchelkanova A Y and Treger D M 2001 Spintronics: a spin-based electronics vision for the future *Science* **294** 1488–95
- [24] Žutić I, Fabian J and Das Sarma S 2004 Spintronics: fundamentals and applications *Rev. Mod. Phys.* **76** 323–410
- [25] Ryan P, Winarski R P, Keavney D J, Freeland J W, Rosenberg R A, Park S and Falco C M 2004 Enhanced magnetic orbital moment of ultrathin Co films on Ge(100) *Phys. Rev. B* **69** 054416
- [26] Mello K E, Murarka S P, Lu T M and Lee S L 1997 Texture analysis of CoGe₂ alloy films grown heteroepitaxially on GaAs(100) using partially ionized beam deposition *J. Appl. Phys.* **81** 7261–7
- [27] Dhar S and Kulkarni V N 1998 Atomic transport in Cu/Ge and Co/Ge systems during ion-beam mixing *Thin Solid Films* **333** 20–4
- [28] Goldfarb I and Briggs G A D 2000 Surface studies of phase formation in Co–Ge system: reactive deposition epitaxy versus solid-phase epitaxy *J. Mater. Res.* **16** 744–52
- [29] Tsay J S, Nieh H Y, Yao Y D, Chen Y T and Cheng W C 2004 Magnetic phases of Co/Ge(111) studied using surface magneto-optic Kerr effect *Surf. Sci.* **566** 226–30
- [30] Sun H P, Chen Y B, Pan X Q, Chi D Z, Nath R and Foo Y L 2005 Formation and evolution of epitaxial Co₅Ge₇ film on Ge(001) surface by solid-state reaction in an *in situ* ultrahigh-vacuum transmission electron microscope *Appl. Phys. Lett.* **87** 211909
- [31] Chang H W, Tsay J S, Chiou Y L, Huang K T, Chan W Y and Yao Y D 2006 Magnetic properties of ultrathin Co/Ge(111) film with oxygen surfactant *J. Appl. Phys.* **99** 08J705
- [32] Sell K, Kleibert A, Oeynhausen V V and Meiwes-Broer K H 2007 The structure of cobalt nanoparticles on Ge(001) *Eur. Phys. J. D* **45** 433–7
- [33] Park K, An C H, Lee M S, Yang C W, Lee H J and Kim H 2009 Microstructural evolution and electrical characteristics of Co-germanide contacts on Ge *J. Electrochem. Soc.* **156** H229–32
- [34] De Keyser K, Van Meirhaeghe R L, Detavernier C, Jordan-Sweet J and Lavoie C 2010 Texture of cobalt germanides on Ge(100) and Ge(111) and its influence on the formation temperature *J. Electrochem. Soc.* **157** H395–404
- [35] Muzychenko D A, Schouteden K, Houssa M, Savinov S V and Van Haesendonck C 2012 Noninvasive embedding of single Co atoms in Ge(111) 2 × 1 surfaces *Phys. Rev. B* **85** 125412
- [36] Barth J V, Brune H, Ertl G and Behm R J 1990 Scanning tunneling microscopy observations on the reconstructed Au(111) surface: atomic structure, long-range superstructure, rotational domains, and surface defects *Phys. Rev. B* **42** 9307–18
- [37] Schouteden K, Lijnen E, Muzychenko D A, Ceulemans A, Chibotaru L F, Lievens P and Van Haesendonck C 2009 A study of the electronic properties of Au nanowires and Au nanoislands on Au(111) surfaces *Nanotechnology* **20** 395401
- [38] Schouteden K, Muzychenko D A, Lievens P and Van Haesendonck C 2009 Low-temperature scanning tunneling microscopy and spectroscopy investigation of the electronic surface state of self-organized Cr islands on Au(111) *J. Nanosci. Nanotechnol.* **9** 6767–71

- [39] Horcas I, Fernandez R, Gomez-Rodriguez J M, Colchero J, Gomez-Herrero J and Baro A M 2007 WSxM: a software for scanning probe microscopy and a tool for nanotechnology *Rev. Sci. Instrum.* **78** 013705
- [40] Muzychenko D A, Savinov S V, Mantsevich V N, Maslova N S, Panov V I, Schouteden K and Van Haesendonck C 2010 Low-temperature scanning tunneling microscopy and spectroscopy of spatial oscillations in the density of states near domain boundaries at the Ge(111)-(2 × 1) surface *Phys. Rev. B* **81** 035313
- [41] Pandey K C 1981 New π -bonded chain model for Si(111)2 × 1 surface *Phys. Rev. Lett.* **47** 1913–7
- [42] Northrup J E and Cohen M L 1983 Atomic geometry and surface-state spectrum for Ge(111)2 × 1 *Phys. Rev. B* **27** 6553–6
- [43] Feenstra R M and Slavin A J 1991 Scanning tunneling microscopy and spectroscopy of cleaved and annealed Ge(111) surfaces *Surf. Sci.* **251** 401–7
- [44] Feenstra R M, Meyer G, Moresco F and Rieder K H 2001 Buckling and band gap of the Ge(111)2 × 1 surface studied by low-temperature scanning tunneling microscopy *Phys. Rev. B* **64** 081306
- [45] Takeuchi N, Selloni A, Shkrebtii A I and Tosatti E 1991 Structural and electronic properties of the (111)2 × 1 surface of Ge from first-principles calculations *Phys. Rev. B* **44** 13611–7
- [46] Einaga Y, Hirayama H and Takayanagi K 1998 Role of 2 × 1 domain boundaries on the transition from 2 × 1 to 2 × 8 at Ge(111) surfaces *Phys. Rev. B* **57** 15567–71
- [47] Uberuaga B P, Leskovar M, Smith A P, Jónsson H and Olmstead M 2000 Diffusion of Ge below the Si(100) surface: theory and experiment *Phys. Rev. Lett.* **84** 2441–4
- [48] Lin D S, Miller T and Chiang T C 1992 Si indiffusion on Ge(100)2 × 1 studied by core-level photoemission *Phys. Rev. B* **45** 11415–8
- [49] Smith G A, Luo L, Hashimoto S, Gibson W M and Lewis N 1989 Room-temperature study of cobalt metal growth on Ge(111) *J. Vac. Sci. Technol. A* **7** 1475–8
- [50] Garleff J K, Wenderoth M, Sauthoff K, Ulbrich R G and Rohlfing M 2004 2 × 1 reconstructed Si(111) surface: STM experiments versus *ab initio* calculations *Phys. Rev. B* **70** 245424